Astronomy & Astrophysics manuscript no.
(will be inserted by hand later)

Dust trapping in thin-ringed protoplanetary disks

C.P. Dullemond[1], T. Birnstiel[2], N. Troncoso[3], L. Perez[3], S. Andrews[4], A. Isella[5], J. Huang[4], Z. Zhu[6], V. Guzmán[7], M. Benisty[8], J. Carpenter[9]

(1) Zentrum für Astronomie, Heidelberg University, Albert Ueberle Str. 2, 69120 Heidelberg, Germany
(2) **XXXX** (3) **XXXX** (4) **XXXX** (5) **XXXX** (6) **XXXX**

July 27, 2018

Abstract. A large fraction of the protoplanetary disks observed with the ALMA Large Programme DSHARP display multiple well-defined and nearly perfectly circular rings in the continuum, in many cases with substantial peak-to-valley contrast. Several of these rings are very narrow in radial extent. In this paper we analyze these results using the assumption that these dust rings are caused by dust trapping in radial pressure bumps. We model this process in a 1-D axisymmetric way, initially with a simple analytic model, then with a more detailed numerical model. We find that ..... **CONCLUSIONS**

Key words. accretion, accretion disks – circumstellar matter – stars: formation, pre-main-sequence – infrared: stars

1. Introduction

The concept of dust trapping in local pressure maxima has become a central theme in studies of planet formation and protoplanetary disk evolution, because it might provide an elegant solution to several problems in these fields of study. Theories of planet formation are plagued by the "radial drift barrier": the problem that, as dust aggregates grow by coagulation, they tend to radially drift toward the star before they reach planetsimal size (e.g. Birnstiel et al. 2010). A natural solution to this problem could be the trapping of dust particles in local pressure maxima (Whipple 1972; Kretke & Lin 2007; Barge & Sommeria 1995; Klahr & Henning 1997). Not only does this process prevent excessive radial drift of dust particles, it also tends to concentrate the dust into small volumes and high dust-to-gas ratios, which is beneficial to planet formation. From an observational perspective, the radial drift problem manifests itself by the presence of large grains in the outer regions of protoplanetary disks (Testi et al. 2003; Andrews et al. 2009), which appears to be in conflict with theoretical predictions (Brauer et al. 2007). One possible solution to this observational conundrum could be that the disks are much more massive in the gas than previously suspected, leading to a higher gas friction for millimeter grains and thus longer drift time scales (Powell et al. 2017). Another explanation is to invoke dust traps. The most striking observational evidence for dust trapping seems to come from large transitional disks, which feature giant dust rings, sometimes lopsided, in which large quantities of dust appears to be concentrated (Casassus et al. 2013; van der Marel et al. 2013). These observations appear to be well explained by the dust trapping scenario Pinilla et al. (2012a). But these transitional disks seem to be rather violent environments, possibly with strong warps (Marino et al. 2015; Benisty et al. 2017) and companion-induced spirals (Dong et al. 2016). For more "normal" protoplanetary disk the dust traps would have to be more subtle. Pinilla et al. (2012b) explored the possibility that the disk contains many axisymmetric local pressure maxima, and calculated how the dust drift and growth would behave under such conditions. It was found that, if the pressure bumps are strong enough, the dust trapping can keep a sufficient fraction of the dust mass at large distances from the star to explain the observed dust millimeter flux. It would leave, however, a detectable pattern of rings that should be discernable with ALMA observations. Since the multi-ringed disk observation of HL Tau (ALMA Partnership et al. 2015) a number of such multi-ringed disks have been detected (Andrews et al. 2016; Isella et al. 2016; Cieza et al. 2017; Fedele et al. 2017, 2018). It is therefore very tempting to see also these multi-ringed disks as evidence for dust trapping, and as an explanation for the retention of dust in the outer regions of protoplanetary disks.

The data from the ALMA Large Programme DSHARP (**REFERENCES**) offers an exciting new opportunity to put this concept to the test, and to put constraints on the physics of dust trapping in axisymmetric pressure maxima. This is an opportunity which we explore in this paper.

If we assume that the rings seen in our data are caused by dust trapping, the question arises: what constraints do the data impose on the physics of dust trapping? To

Source	d [pc]	$M_*/M_\odot$	$L_*/L_\odot$
AS 209	121	0.832	1.413
Elias 24	136	0.776	6.03
HD 163296	101	2.04	17.0
GW Lup	155	0.457	0.331
HD 143006	165	1.78	3.80

Table 1. The stellar parameters assumed for the stars studied in this paper. Distance is in parsec and mass and luminosity are in units of the solar values.

explore this we start by studying the rings individually, assuming that the dust does not escape from the ring. This makes it possible to look for a steady-state dust trapping solution in which the radial drift forces (that push the dust to the pressure peak) are balanced by turbulent mixing (that tends to smear out the dust away from the pressure peak). In Section A we will construct a very simplified analytic dust trapping model, and confront this with the most well-isolated rings from our sample. **Describe the next sections.** But before we do the modeling, we review, in Section 2, the key aspects of the data from our ALMA Large Programme that we compare to our models.

2. The high-contrast rings of AS 209, Elias 24, HD 163296, GW Lup and HD 143006

In this paper we focus on those sources of the DSHARP Programme that show high-contrast and radially thin rings that are separated by deep valleys, and that are sufficiently face-on to not have to worry about 3-D line-of-sight issues. These are AS 209, Elias 24, HD 163296, GW Lup and HD 143006. Their stellar parameters are given in Table 1.

A gallery of these sources is shown in Fig. 1. For an overview of the ALMA Large Programme we refer to **Andrews et al. XXXX**, and for an in-depth discussion on the data of the individual sources we refer to [**LIST HERE THE PAPERS**].

The high-contrast rings of these sources provide "clean laboratories" for testing the theory of dust trapping in a ring-by-ring manner. Fig. 2 shows the radial profile (deprojected for inclination) of the thermal emission of the dust of the five disks. The procedure used to extract these radial profiles from the continuum maps is described in [**Paper Jane Huang, but note that for HD 163296 and HD 143006 we removed the blob**]. The brightness is expressed as linear brightness temperature $T_{\rm br,lin} = (c^2/2k_B)I_\nu/\nu^2$, where I_ν is the intensity, c the light speed, k_B the Boltzmann constant, and ν the frequency[1].

[1] It should be noted that the full (non-linear) brightness temperature, defined such that $B_\nu(T_{\rm br,full}) = I_\nu$, with $B_\nu(T)$ the Planck function, can have very different values, in particular at low brightness. As a result $T_{\rm br,full}(r)$ tends to vastly underestimate the contrast between the rings and the inter-ring regions. Therefore, in this paper we plot the brightness using the linear brightness temperature, which is proportional to the intensity in Jy/beam.

As is shown in Appendix A, for a Gaussian pressure bump the solution to the radial dust mixing and drift problem is, to first approximation, also a Gaussian, with a width smaller than, or equal to, that of the gas pressure bump. Our analysis of the eight rings of this paper therefore naturally starts with the fitting of the observed radial intensity profiles with a Gaussian function. For some [**CHECK**] of the rings of this paper such Gaussian fits were done in the context of fitting the entire radial intensity profile in the uv-plane to the ALMA data (**Guzman et al.XXXX; More??**). Our fits may deviate slightly from those [**CHECK**], because here we put emphasis on the shape of the peak of the rings, and deemphasize the wings.

The fitting procedure is described in Appendix B. The fitting was done in the image plane, in order to make it possible to fit to a limited radial range, i.e. selecting a single ring. The Gaussian fits are shown as inverse parabolas in Fig. 2. In Fig. 3 these Gaussian fits are shown in close-up. The parameters of the best fits are listed in Table 2.

The observed rings are the result of the thermal emission of a dust ring convolved with the ALMA beam. The standard deviation width σ of the fitted Gaussian profile is given in Table 2. To obtain the width of the underlying dust ring we have to deconvolve. Assuming a Gaussian beam and a Gaussian dust ring, we can use the rule of the convolution of two Gaussians, and obtain the width w_d of the dust ring

$$w_d = \sqrt{\sigma^2 - b^2} \tag{1}$$

where b is the beam width expressed as standard deviation in units of au ($b = d_{\rm pc} b_{\rm fwhm,as}/2.355$, where $b_{\rm fwhm,as}$ is the beam full width at half maximum in units of arcseconds, and $d_{\rm pc}$ is the distance to the source in units of parsec). The width of the dust rings in units of the local pressure scale height h_p (see Table 2) can only be roughly estimated, because we do not know the disk midplane temperature. Our estimate is made as follows:

$$T_{\rm d}(r) = \left(\frac{\frac{1}{2}\varphi L_*}{4\pi r^2 \sigma_{\rm SB}}\right)^{1/4} \tag{2}$$

where $\sigma_{\rm SB}$ is the Stefan-Boltzmann constant and φ is the so-called flaring angle (e.g. Chiang & Goldreich 1997; D'Alessio et al. 1998; Dullemond et al. 2001). The pressure scale height then follows from $h_p = \sqrt{k_B T_{\rm d} r^3/\mu m_p G M_*}$ with k_B the Boltzmann constant, m_p the proton mass, G the gravitational constant and $\mu = 2.3$ the mean molecular weight in atomic units. The stellar parameters are taken from Table 1. We take the flaring angle to be $\varphi = 0.02$ which is an estimate based on typical values from models. But this value can easily be wrong by a factor of four or so. The fact that the pressure scale height goes as $T_{\rm d}^{1/2} \propto \varphi^{1/8}$ means, however, that such an error only affects h_p mildly.

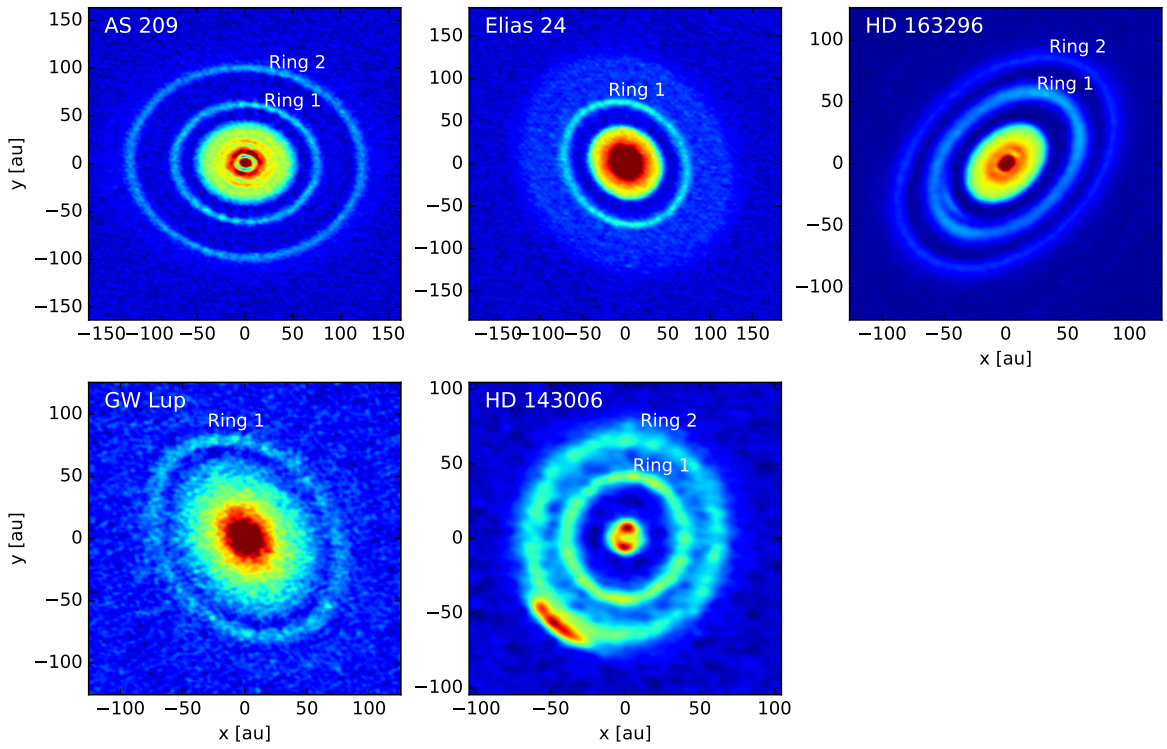

Fig. 1. The continuum maps in band 6 of the five disks in our sample which have the most pronounced rings. The eight highest contrast rings, which are the topic of this paper, are marked in the images. For a detailed description of these data, see **Guzmán et al. (2018)** for AS 209, **XXXX**

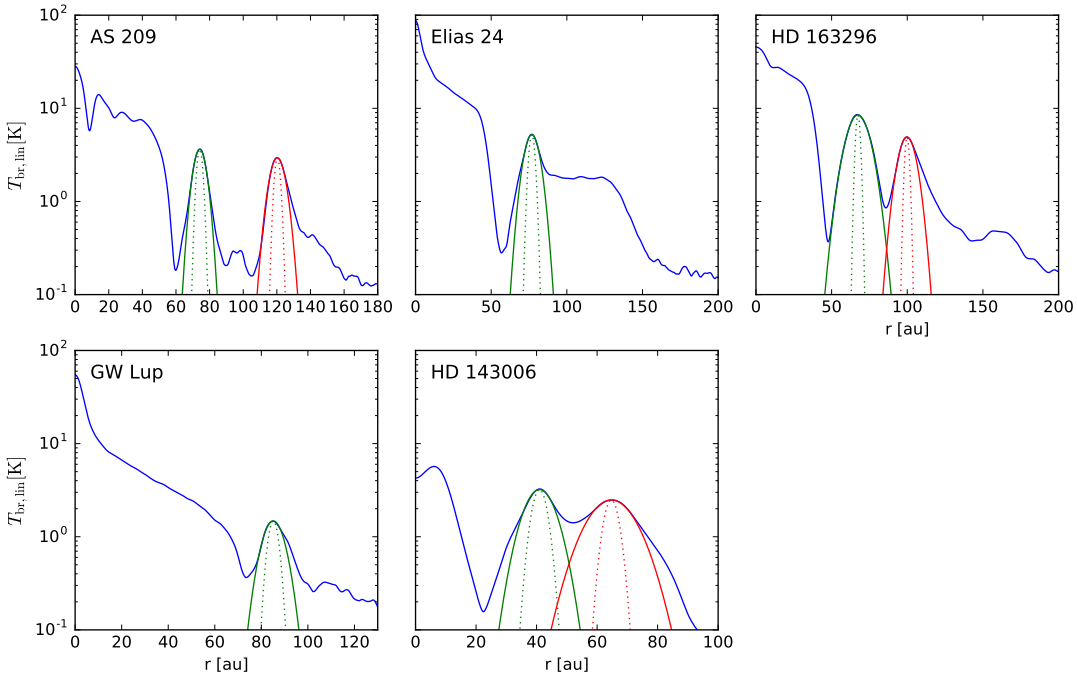

Fig. 2. The linear brightness temperature in band 6 of the five disks in our sample which have the most pronounced rings. The vertical axis is logarithmic to better show the contrast. The eight highest contrast rings are fitted by a Gaussian profile, shown as the solid inverse parabolas. The dotted inverse parabolas are Gaussians with the width of the ALMA beam. For a detailed description of these data, see **Guzmán et al. (2018)** for AS 209, **XXXX**

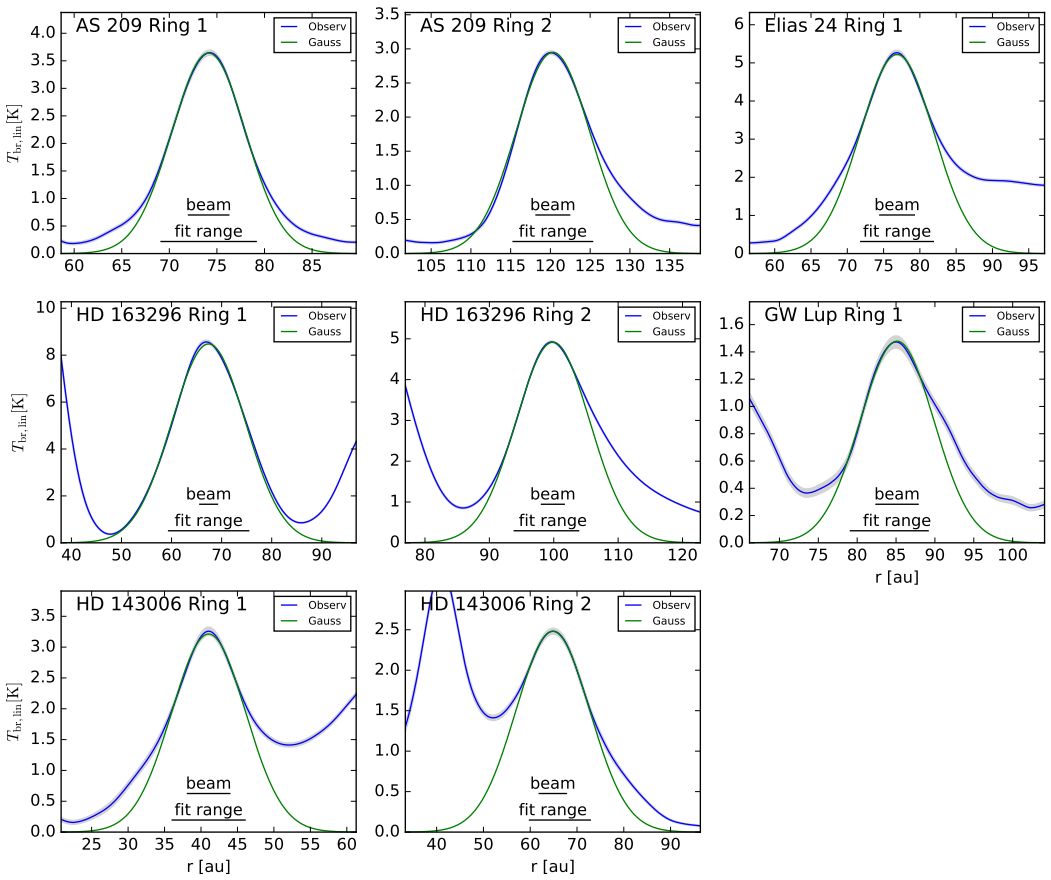

Fig. 3. Gaussian fits to the eight rings of this paper. The blue curves are the observations, the green curves are the best fit Gaussian profiles. The "fit range" bar shows the radial range within which the Gauss was fitted to the data. The fit range was chosen to fit the part of the curve that, by eye, most resembles a Gaussian. The "beam" bar shows the FWHM beam size of the observations. The grey band around the blue curve shows the estimated uncertainty of the data.

We see from Table 2 that some rings are narrower than the (estimated) pressure scale height h_p, while others are broader. This comparison is important because long-lived pressure bumps in the gas cannot be radially narrower than about one pressure scale height. If a thermal emission ring produced by the dust is substantially narrower than h_p, then some kind of dust trapping must have taken place. If this were not the case, then the dust emission profile would have the same shape as the gas midplane density, and thus the gas midplane pressure bump would then be a narrower than h_p.

We see that 5 out of 8 rings are narrower than h_p, but not by much. None are less than half the width of the pressure scale height of the gas. This is perhaps slightly disappointing, because it means that these results are no irrefutable proof that dust trapping is playing a role in the shaping of these rings. But it is strong evidence for that nonetheless.

For these observations the fwhm beam size is of the order of 35 milliarcseconds [**CHECK AND MAKE MORE ACCURATE**]. This number can be compared to the fwhm ring width in Table 2, and it shows that the widths of all the rings are spatially resolved. Some are only marginally resolved (AS 209 rings 1 and 2, GW Lup and the ring 1 of HD 143006), but the data are inconsistent with radially unresolved rings. This is confirmed by more detailed analysis in the uv-plane (**REFS TO Guzmán et al. (2018)**).

These Gaussian profiles fit the observed data remarkably well, as can be best seen in Fig. 3. For the broad rings of HD 163296 the closeness to a Gaussian profile is particularly striking, given that these rings are resolved by many beam widths. In particular in this source there is therefore no doubt that the Gaussian profile is a reflection of a real phenomenon, and is not caused by unknown observational or data reduction issues. But also the rings of AS 209, while not as well-resolved as those of HD 163296, are remarkably close to Gaussian.

For Elias 24 the ring fits a Gaussian near the peak, but deviates from Gaussian already less half a width from

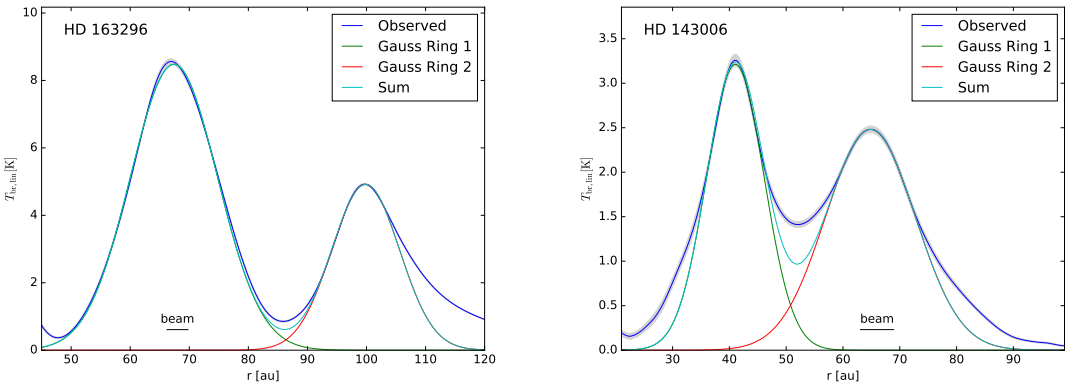

Fig. 4. The sum of the two Gaussian fits for the two sources with two partly overlapping rings: HD 163296 and HD 143006.

Source	Ring	$r_{\rm in}$ [au]	$r_{\rm out}$ [au]	A [K]	r_0 [au]	fwhm [mas]	σ [au]	w_d [au]	$T_{\rm d}$ [K]	$T_{\rm d,br,lin}$ [K]	w_d/h_p	τ	$M_{\rm d,ri}$ [$M_\oplus$]	$M_{\rm d,iv}$ [$M_\oplus$]
AS 209	1	69	79	3.64	74.13	75.42	3.88	3.43	15.8	10.9	0.6	0.41	33.3	1.81
AS 209	2	115	125	2.95	120.31	90.28	4.64	4.28	12.4	7.7	0.4	0.48	74.3	4.04
Elias 24	1	72	82	5.22	76.85	87.99	5.08	4.66	22.3	17.2	0.6	0.36	41.1	2.23
HD 163296	1	60	76	8.48	67.41	171.73	7.36	7.21	30.8	25.6	1.7	0.40	56.9	3.09
HD 163296	2	94	104	4.92	99.86	133.56	5.73	5.53	25.3	20.2	0.8	0.28	48.3	2.62
GW Lup	1	79	89	1.48	85.13	72.08	4.74	4.15	10.3	5.7	0.6	0.30	36.3	1.97
HD 143006	1	35	45	3.21	41.05	72.20	5.06	4.42	27.2	22.0	2.1	0.16	10.5	0.57
HD 143006	2	59	72	2.48	64.83	112.51	7.88	7.49	21.6	16.6	2.0	0.16	26.5	1.44

Table 2. The model parameters for the Gaussian ring fits in Figs. 2 and 3. The values $r_{\rm in}$ and $r_{\rm out}$ are the inner and outer boundary of the fitting domain. A is the peak linear brightness temperature of the best-fit Gaussian ring model, r_0 is its radius in au, fwhm is the width expressed as full-width-at-half-maximum in units of milliarcsecond, σ is its width expressed as standard deviation in units of au and w_d is the width of the underlying (deconvolved) dust emission profile, also expressed as standard deviation in units of au. The last six columns are derived from a simple disk model assumption: $T_{\rm d}$ is the midplane temperature of the disk (we assume gas and dust temperature to be equal) computed from Eq. (2) assuming a flaring angle of $\varphi = 0.02$. From that one can derive the corresponding linear brightness temerature $T_{\rm d,br,lin} = B_\nu(T_{\rm d})c^2/2\nu^2$ where $\nu = c/0.13\,{\rm cm}$ is the frequency belonging to the wavelength of 0.13 cm of ALMA band 6. The fourth-to-last column expresses the deconvolved dust ring width in units of the disk pressure scale height h_p computed from $T_{\rm d}$. The τ column gives the estimated optical depth at the peak of the ring, calculated from $\tau = -\ln(1 - A/T_{\rm d,br,lin})$. The last two columns are the computed dust mass in the ring in units of Earth masses, assuming the small grain absorption opacity $\kappa_{\rm abs,ri}(\lambda = 0.13\,{\rm cm}) = 1.70\,{\rm cm}^2/{\rm g}$ of Ricci et al. (2010) ($M_{\rm d,ri}$) and the corresponding value $\kappa_{\rm abs,ri}(\lambda = 0.13\,{\rm cm}) = 31.3\,{\rm cm}^2/{\rm g}$ of Ivezic et al. (1997) ($M_{\rm d,iv}$). In making these estimates, the optically thin approximation was used. See Appendix C for details. An estimate of the optical-depth-corrected dust mass can be made by multiplying the mass values in the table by $\tau/(1 - e^{-\tau})$.

the center. Likewise for the rings of HD 143006. The ring around GW Lup is an intermediate case, which fits a Gauss well on the inner flank, but rather badly on the outer flank.

In all ring profiles shown in Fig. 3 the observed profile rises above the Gaussian fit at some point in the wings. For the inner flanks of ring 1 of Elias 24 and ring 1 of HD 143006, as well as for the outer flanks of ring 2 of AS 209, ring 2 of HD 163296, the ring of GW Lup and ring 2 of HD 143006 the excess above the Gaussian gradually increases away from the peak of the Gaussian. Put differently, the profiles appear to deviate from Gaussian shape to pyramid-shape (or Lorenzian shape) in the flanks. This cannot be simply the addition of a constant background, because that would preserve the Gaussian shape, and merely lift it higher. Instead, while the core of the profile can clearly be well-described by a Gaussian, in the flanks there is a clear transition to a different, wider, shape.

A similar effect occurs between the two rings in HD 163296 and HD 143006, where in particular for HD 143006 it is clear from Fig. 4 that it cannot be just the effect of the sum of the two Gaussians.

It is not immediately clear whether this is relevant or just chance. It lies in the nature of fitting a Gaussian profile to something non-Gaussian that there will be a region close to the peak where the curve fits the Gaussian rea-

sonably well, while the deviation will increase the farther away from the peak one looks. This danger is particularly large in the present case, since the fitting range was chosen to maximize the similarity to the Gauss near the peak. Nevertheless, it clearly signals a deviation from Gaussian.

Given the closeness of the profiles to a Gaussian, we can use the Gaussian fit to make estimates of the total mass of dust trapped in each of these rings. The procedure is described in Appendix C, and the results, for the two opacity choices we make, are listed in Table 2. In making these estimates we have assumed the dust to be made up of micron-sized dust, which is likely too small. The mass based on the Ivezic opacity, $M_{\rm d,iv}$, will increase for $a > \lambda/2\pi$ by a factor of $2\pi\, a/\lambda$ with $\lambda = 0.13\,$cm. For the mass based on the Ricci opacity the factor first decreases when a approaches the opacity peak around $a = \lambda/2\pi$ and then increases for $a > \lambda/2\pi$. Both behaviors can be seen as the inverse behavior of the opacities shown in Fig. C.1. For ever increasing grain size estimate, the mass estimate will increase indefinitely for both opacity choices.

3. The rings as dust traps

Given the well separated narrow rings in the above sources, we can analyze these rings on a one-by-one basis. The hypothesis we are going to test is that the rings are caused by dust trapping in axisymmetric pressure bumps. For simplicity we will assume that the radial gas pressure profile is fixed in time, and there is no back reaction of the dust onto the gas. The pressure bump is assumed to be so strong that the dust trapping in these rings is nearly perfect: no dust escapes. We then expect that the dust distribution finds an equilibrium between dust drift and turbulent spreading. Low turbulence will lead to thinner dust rings than high turbulence. For simplicity we shall assume the gas pressure bump to have a Gaussian radial profile with its peak at radius r_0 and width $w \ll r_0$. This problem can be solved analytically.

3.1. Model

Consider the following radial Gaussian profile for the pressure at the disk midplane:

$$p(r) = p_0 \exp\left(-\frac{(r-r_0)^2}{2w^2}\right) \tag{3}$$

We will discuss the hydrodynamic stability of a gas distribution arranged in this way in Section A.5. But for now we will not be concerned with that and we will assume the pressure-profile of Eq. (3) to be given and fixed.

In Appendix A we derive that, for our purposes, a good approximation of the stationary dust distribution within the dust trap is:

$$\Sigma_{\rm d}(r) = \Sigma_{\rm d0} \exp\left(-\frac{(r-r_0)^2}{2w_{\rm d}^2}\right) \tag{4}$$

where

$$w_{\rm d} = w\,\left(1+\psi^{-2}\right)^{-1/2} \tag{5}$$

with ψ given by

$$\psi = \sqrt{\frac{\alpha_{\rm turb}}{\rm Sc\,St}} \tag{6}$$

Here St is the Stokes number of the dust particles (Eq. A.3), Sc is the Schmidt number of the turbulence in the gas, and $\alpha_{\rm turb}$ is the usual turbulence parameter. Note that this solution is for a single grain size.

For large grains and/or weak turbulence one finds $\psi \ll 1$, which leads to $w_{\rm d} \ll w$. In this case the dust is strongly trapped near the peak of the pressure bump. The opposite is the case for small grains and/or strong turbulence, for which one gets $\psi \gg 1$, which leads to $w_{\rm d} \to w$. In this case the trapping is very weak and the dust-to-gas ratio within the pressure bump stays constant. Only in the very wings of the Gaussian pressure bump is dust trapping significant, but this effect can only be studied using the more accurate non-gaussian solution of Eq. (A.13). We will return to the dust trapping effect in the wings in Section **XXXXX**.

Eq. (4) has only two parameters: $\Sigma_{\rm d0}$ and $w_{\rm d}$. Both can be fairly directly measured from the observations, though $\Sigma_{\rm d0}$ will depend on the opacity, and hence on the unknown grain size (see discussion in Appendix C). The values of $w_{\rm d}$ for the rings in our sample can be directly taken from Table 2.

The width of the dust ring $w_{\rm d}$ is physically set by $\alpha_{\rm turb}$, Sc, St and w through the above equations. We therefore have one observational value for four unknown parameters. This is heavily degenerate. All we can do is to test if the measured value of $w_{\rm d}$ is consistent with expected values of $\alpha_{\rm turb}$, Sc, St and w.

3.2. Ranges of $\alpha_{\rm turb}$, Sc, St and w

Reasonable values of $\alpha_{\rm turb}$, Sc, St and w obey certain restrictions. First of all, the Schmidt number Sc is merely a way to relate the turbulent viscosity with the turbulent mixing. If we do not strive to learn about the turbulent viscosity, and instead are satisfied with learning only about the turbulent mixing, then we are only interested in the combination $\alpha_{\rm turb}/{\rm Sc}$. For simplicity we set ${\rm Sc} = 1$.

The value of the turbulence parameter $\alpha_{\rm turb}$ is usually considered to be between $10^{-6} \lesssim \alpha_{\rm turb} \lesssim 10^{-2}$.

The width of the pressure bump cannot be smaller than about a pressure scale height, but also not smaller than the width of the dust ring. Therefore $w_{\rm min} = \max(h_p, w_{\rm d})$. In the case of the double rings (AS 209, HD 163296 and HD 143006), the full-width-at-half-maximum $2.355\,w$ should not exceed the radial separation of the rings. For the two single ring sources we take the deepest point of the gap to the inside of the ring as the upper limit on the half-width-at-half-maximum $1.178\,w$. These lower and upper limits on w are listed in Table 3.

The Stokes number St can be any value. But it is directly related to the grain size a and the gas density $\rho_{\rm g}$, where the gas density is directly related to the gas surface density $\Sigma_{\rm g}$ via $\Sigma_{\rm g} = \sqrt{2\pi} h_p \rho_{\rm g}$. If we have observational constraints on a and a good estimate of the gas surface

density $\Sigma_{\rm g}$, then we can eliminate this uncertainty, and we are left with two unknown parameters ($\alpha_{\rm turb}$ and w) for one measurement ($w_{\rm d}$). Unfortunately, while estimating a from observations may be doable, it is far more difficult to estimate $\Sigma_{\rm g}$. Standard disk gas mass estimates are of limited use, as they are based on measuring the dust mass and multiplying it by the estimated gas-to-dust ratio. Since we are testing the hypothesis of dust trapping, we cannot assume a standard gas-to-dust ratio.

One can, however, set an upper bound on $\Sigma_{\rm g}$ by demanding that the disk is gravitationally stable, i.e. that the Toomre parameter obeys

$$Q_{\rm Toomre} \equiv \frac{c_s \Omega_K}{\pi G \Sigma_{\rm g}} > 2 \tag{7}$$

Here $c_s = \sqrt{k_B T/\mu m_p}$ is the isothermal sound speed, with k_B the Boltzmann constant, m_p the proton mass, and $mu = 2.3$ the mean molecular weight in atomic units. $\Omega_K = \sqrt{GM_*/r^3}$ is the Kepler frequency, G is the gravitational constant and, finally, $\Sigma_{\rm g}$ the gas surface density. Taking the disk midplane temperature from Table 2, which was calculated using Eq. (2), we can compute the upper limits on $\Sigma_{\rm g}$ for all of the rings. The results are given in Table 3.

One can estimate a lower limit to the gas density by demanding that the gas surface density must be at least as large as the dust surface density, since dust trapping is unlikely to achieve a larger concentration of dust than that. Depending on which of the two opacities we use (see Appendix C) we arrive at different estimates of $\Sigma_{\rm d}(r = r_0)$. By demanding $\Sigma_{\rm g} \gtrsim \Sigma_{\rm d}$ we arrive at two lower limits of the gas surface density, given in Table 3. It is likely that even for much larger values of the gas surface density the dust-gas mixture becomes unstable to the streaming instability and other types of instabilities. If we can convince ourselves that such instabilities are not operating in these rings, then this puts a substantially stronger (i.e. larger) lower limit on the gas surface density.

Also if the grains are much larger than $\lambda/(2\pi) \simeq 0.02\,$cm, the opacity drops and the resulting dust surface density estimate increases, yielding larger lower limits to the gas density.

Along this line of thinking one can compute the largest grain radius for which the Toomre parameter of the disk stays above 2. We use the Ivezic opacity for that, which, for large grains, has similar values as the Ricci opacity. This leads to values of several centimeters to half a meter (Table 3). Again these are conservative limits, with real values likely to be substantially smaller.

3.3. Application to the observed rings

We now wish to apply the model of Subsection 3.1 with the limits on the parameter ranges derived in Subsection 3.2 to the observed ring widths w_d listed in Table 2.

From an assumed value of w and the measured value $w_{\rm d}$ we can directly compute the ratio $\alpha_{\rm turb}/{\rm St}$

$$\frac{\alpha_{\rm turb}}{\rm St} \equiv \psi^{-2} = \left[\left(\frac{w}{w_{\rm d}} \right)^2 - 1 \right]^{-1} \tag{8}$$

where we used Eqs. (5, 6), and set ${\rm Sc} = 1$. We will consider two choices of w: the $w_{\rm min}$ and $w_{\rm max}$ from Table 3.

For the choice $w = w_{\rm max}$ (the widest possible pressure bump) the dust rings are all narrower that the gas rings: $w_{\rm d} < w$, which implies that the dust trapping is operational, and Eq. (8) gives information about the turbulent strength. For the choice $w = w_{\rm min}$ (the narrowest possible pressure bump) we can only use Eq. (8) for the rings for which $w_{\rm d} < h_p$. The reason is that for those rings with $w_{\rm d} > h_p$ (marked with a * in Table 3) the minimal pressure bump width is $w_{\rm min} = w_{\rm d}$, and the dust ring is as wide as the pressure bump, implying that dust trapping is weak or non-operational. Any increase of $\alpha_{\rm turb}/{\rm St}$ will keep $w_{\rm d} = w_{\rm min}$, so one cannot derive any value for $\alpha_{\rm turb}/{\rm St}$. But for other rings we can compute $\alpha_{\rm turb}/{\rm St}$. The resulting values for both choices of pressure bump width are given in Table 3. They can be understood as the lower and upper limit on $\alpha_{\rm turb}/{\rm St}$.

The next task is to convert from Stokes number St to grain size a. The Epstein regime is valid for the typical grains we are interested in (less than a meter in size), in which case a and St are related by

$${\rm St} = \frac{\pi}{2} \frac{\xi_{\rm dust} a}{\Sigma_{\rm g}} \tag{9}$$

where $\Sigma_{\rm g}$ is the gas surface density and $\xi_{\rm dust}$ is the material density of the dust grains. Given that grains are expected to be a mixture of silicate, amorphous carbon and water ice, a value of $\xi_{\rm dust} \simeq 2\,{\rm g/cm^3}$ is reasonable.

To get a feeling for the results, let us choose the grain size to be $a = 0.02\,$cm, which corresponds to $\lambda/2\pi$ for $\lambda = 0.13\,$cm (the wavelength of ALMA band 6). The corresponding Stokes numbers, for the most massive possible gas disk ($\Sigma_{\rm g} = \Sigma_{\rm g,max}$), are listed in Table 3. This then allows us to convert the value of $\alpha_{\rm turb}/{\rm St}$ into a value of $\alpha_{\rm turb}$. For the case $w = w_{\rm max}$ this leads to values $\alpha_{\rm turb} = 10^{-4} \cdots$ few $\times 10^{-3}$, listed in Table 3 (column $\alpha_{\rm exmp}$).

These low values of $\alpha_{\rm turb}$ are consistent with the low values or upper limits reported recently (Pinte et al. 2016; Flaherty et al. 2018) [**more?**]. However, it has to be kept in mind that the values of $\alpha_{\rm turb} = \alpha_{\rm exmp}$ were derived for an example choice of parameters: : $w = w_{\rm max}$, $\Sigma_{\rm g} = \Sigma_{\rm g,max}$ and $a = 0.02\,$cm. For a smaller value of w, a lower value of $\Sigma_{\rm g}$, or larger grains, the computed value of $\alpha_{\rm turb}$ will increase. So that it is hard to set a true upper limit on $\alpha_{\rm turb}$ from these observations.

This seems to be in conflict with the results found by Pinte et al. (2016) who, from measuring an upper limit on the vertical extent of the dust, imply an upper limit on $\alpha_{\rm turb}$ of 3×10^{-3}. [**IMPORTANT: We have to find out**

Source	Ring	$w_{\rm min}$ [au]	$w_{\rm max}$ [au]	$\Sigma_{\rm g,min,iv}$ [g/cm^3]	$\Sigma_{\rm g,min,ri}$ [g/cm^3]	$\Sigma_{\rm g,max}$ [g/cm^3]	$a_{\rm max}$ [cm]	$\rm St_{(a=0.02\,cm)}$ (for $\Sigma_{\rm g,max}$)	$\alpha/\rm St$ (for $w_{\rm max}$)	$\alpha/\rm St$ (for $w_{\rm min}$)	$\alpha_{\rm exmp}$
AS 209	1	5.59	19.6	1.1e-02	2.0e-01	1.6e+01	15.7	3.9e-03	3.2e-02	6.0e-01	1.2e-04
AS 209	2	10.25	19.6	1.2e-02	2.3e-01	6.9e+00	5.8	9.1e-03	5.0e-02	2.1e-01	4.5e-04
Elias 24	1	7.26	17.1	9.7e-03	1.8e-01	1.8e+01	18.8	3.6e-03	8.0e-02	7.0e-01	2.9e-04
HD 163296	1	7.21*	13.8	1.1e-02	1.9e-01	4.1e+01	40.0	1.5e-03	3.8e-01	–	5.8e-04
HD 163296	2	7.07	13.8	7.8e-03	1.4e-01	2.0e+01	27.3	3.1e-03	1.9e-01	1.6e+00	5.9e-04
GW Lup	1	7.49	9.9	8.3e-03	1.5e-01	7.8e+00	9.8	8.0e-03	2.1e-01	4.4e-01	1.7e-03
HD 143006	1	4.42*	10.1	4.7e-03	8.6e-02	7.5e+01	167.2	8.4e-04	2.4e-01	–	2.0e-04
HD 143006	2	7.49*	10.1	4.8e-03	8.8e-02	3.4e+01	73.2	1.9e-03	1.2e+00	–	2.3e-03

Table 3. Limits on the free parameters of the dust trapping model. The lower limit to the pressure bump width $w_{\rm min}$ is the pressure scale height h_p. If, however, the width of the dust ring $w_d > h_p$, then the lower limit is w_d (marked with the symbol *). The upper limit $w_{\rm max}$ is derived from the separation between the rings (for AS 209, HD 163296 and HD 143006) or from the separation of the ring to the nearest minimum (for Elias 24 and GW Lup). The two lower limits on the gas surface density $\Sigma_{\rm g}$ were derived by demanding $\Sigma_{\rm g} \gtrsim \Sigma_{\rm d}$, where $\Sigma_{\rm d}$ was computed in Appendix C using two different opacities: that of Ivezic et al. (leading to $\Sigma_{\rm g,min,iv}$) and that of Ricci et al. (leading to $\Sigma_{\rm g,min,ri}$). The column marked with $\Sigma_{\rm g,max}$ is the upper limit on the gas surface density derived from demanding that the gas disk is gravitationally stable. The $a_{\rm max}$ column is the maximum grain size for which the derived dust surface density together with the gas surface density remain gravitationally stable. The $\rm St_{(a=0.02\,cm)}$ column gives an example value of the Stokes number: it is the value of St if the grains have a radius of 0.02 cm, for the case of $\Sigma_{\rm g} = \Sigma_{\rm g,max}$. The two columns for $\alpha/\rm St$ are derived for the widest and narrowest gas bump, respectively. The column $\alpha_{\rm exmp}$ is the value of $\alpha_{\rm turb}$ for an example choice of parameters: $w = w_{\rm max}$, $\Sigma_{\rm g} = \Sigma_{\rm g,max}$ and $a = 0.02$ cm.

why Pinte et al. find this limit. Do they have additional constraints? Why can't they increase the grain size indefinitely? What are the constraints Eric and Andrea find for the similar analysis of HD 163296?]

Can we derive a *lower* limit to $\alpha_{\rm turb}$? This depends on whether we have information about the grain size. At present we have only the high resolution data for band 6, so we do not yet have information about the radial profile of the spectral slope. But in several recent observations of the spectral index across ringed disks (ALMA Partnership et al. 2015; Huang et al. 2018) one clearly sees that $\alpha_{\rm spec}$ varies across these rings, being closer to 2 at the ring center and substantially larger between the rings. This makes sense in terms of the dust trapping scenario in which we expect larger grains to be trapped more efficiently (and thus dominate the peak of the ring) than smaller grains, because the smaller grains will be more subject to turbulent mixing. This scenario requires a grain size distribution, so that the width of the dust ring is smaller for the bigger grains and bigger for the smaller ones. We will discuss our model in the context of grain size distributions in Section 3.4. But assuming that future data will also show similar spectral slope changes for our sources, we can already conclude that the grains trapped in the rings must have sizes larger than $\lambda/2\pi = 0.02$ cm. The measured (resolved) width of the dust ring w_d then implies a lower limit to $\alpha_{\rm turb}$. The value $\alpha_{\rm turb} = \alpha_{\rm exmp}$ is then, in fact, this lower limit. We will, however, have to wait until high resolution ALMA data in another band becomes available to verify the minimal grain size of 0.02 cm.

Should the low spectral slope at the peak of the rings be confirmed, then the lower limits on $\alpha_{\rm turb}$ from the $\alpha_{\rm exmp}$ column in Table 3 paint a different picture from the low-turbulence picture that has emerged in recent times. The values of a few times 10^{-4} to a few times 10^{-3} are low, but they are only lower bounds. It would be somewhat unlikely if all rings have parameters at this extreme size of parameter space, and it is therefore likely that $\alpha_{\rm turb}$ is easily a factor of ten higher or so. This would imply that protoplanetary disks are substantially turbulent after all. But to confirm this, we need to dig a bit deeper by including size distributions (Section 3.4) and non-perfect ("leaky") dust traps (Section **XXXX**).

We can make predictions for pressure slopes in CO

CONSIDER PRESSURE OFFSET!

3.4. Including a grain size distribution

[**Here we will move away from a single grain size and see if we can understand the deviations from Gaussian by a grain size distribution**]

4. Streaming instability, clumping, and the spectral index

[**This section is temporarily hidden, because a lot still has to be done on this. Maybe it should be removed and put into a future paper.**]

5. Discussion

5.1. Condition for the streaming instability

In the literature it is often mentioned that the streaming instability requires a dust-to-gas surface density ratio of $\Sigma_{\rm d}/\Sigma_{\rm g} \gtrsim 0.02$ or higher to operate **XXXXXXXX**. This can, however, not be directly compared to our models, because this value of 0.02 was found for models without any pre-determined turbulence. The turbulence in those models was induced by the streaming instability itself or, if the streaming instability does not operate, by the Kelvin-Helmholtz instability (**XXXX**). In the analytic model of this Section, on the other hand, we set the turbulence strength by hand, by setting $\alpha_{\rm turb}$ to some value. In essence, we assume that there is another source of turbulence, such as the magnetorotational instability (**XXXX**) or the vertical shear instability (**XXXX**), that determines the mixing of the dust in the disk.

According to Youdin & Goodman (2005) the true criterion for the onset of the streaming instability is the ratio of dust and gas *volume* densities $\rho_{\rm d}/\rho_{\rm g} \gtrsim 1$. For a given surface density ratio $\Sigma_{\rm d}/\Sigma_{\rm g}$, the midplane volume density ratio, for a single grain species with midplane Stokes number ${\rm St} \ll 1$, depends on the turbulent strength as

$$\frac{\rho_{\rm d}}{\rho_{\rm g}} \simeq \left(1 + \frac{\rm St}{\alpha_{\rm turb}}\right) \frac{\Sigma_{\rm d}}{\Sigma_{\rm g}} \tag{10}$$

The criterion of $\Sigma_{\rm d}/\Sigma_{\rm g} \gtrsim 0.02$ mentioned in the literature thus relates to the criterion $\rho_{\rm d}/\rho_{\rm g} \gtrsim 1$ via the turbulent strength and the Stokes number. Given that we do not compute the turbulent strength but prescribe it, we should rely on the more fundamental volume density criterion of Youdin & Goodman (2005) to assess whether the dust in our model triggers the streaming instability or not.

In our analytic setup of Section **CHECK** the dust ring is about 5 times narrower than the gas bump. Assuming that initially the dust-to-gas ratio was 0.01, this implies a dust-to-gas surface density ratio at the peak of the ring of 0.05, which is in excess of the usual 0.02 value. But as long as ${\rm St} \lesssim 19\alpha_{\rm turb}$, Eq. (10) shows that the midplane volume density ratio still stays below unity and no streaming instability sets in.

5.2. Can a resolved ring be in fact a blend of several unresolved rings?

Measuring the width of rings with finite-resolution observations is, of course, limited to ring widths that are larger than the "beam". However, even for cases where the ring width clearly exceeds the beam size by a factor of a few or more, one may ask the question: is the wide ring we see truly a single wide ring, or could it also be made up of a series of spatially unresolved rings that are blended into a single wide ring due to the beam convolution? This question is particularly relevant for the very wide rings of HD 163296. It is, of course, hard to answer in general, since we have no observational means to test this.

But from the perspective of particle trapping by a pressure bump this question can be rigorously answered. A long-lived radial pressure perturbation in a protoplanetary disk cannot be much narrower than about a pressure scale height $h_p(r)$. A dust ring produced by dust trapping in this pressure bump may become rather narrow, dependent on a variety of parameters, as discussed in Section A. But there can not be more than a single such dust ring in each pressure bump.

For the wide rings of HD 163296 the pressure scale height, even under the most optimistically low disk temperature (e.g. 10 K) the pressure scale height at rings 1 and 2 are 2.4 au and 4.3 au, respectively, which correspond to fwhm widths of 55 and 101 milliarcseconds, respectively (where we have multiplied by 2.355 to obtain the full-width at half-maximum corresponding to a gaussian with h_p as standard deviation width). Clearly the ALMA observations in band 6, with fwhm beam size of 35 mas, spatially resolve the pressure scale height. This means that the ring separation will be spatially resolved by ALMA, ruling out the possibility that the wide rings are made up of a multitude of narrow rings, at least in the dust trapping scenario.

[**Add discussion of the plateau of Elias 24**]

5.3. Interpretation of the millimeter flux in terms of grain size

A common rule of thumb for interpreting millimeter and sub-millimeter fluxes and intensities from thermal dust emission is that you "observe the grain size equal to the wavelength you observe at". This rule is based on the tendency of the dust opacity derived from a Mie calculation to peak at wavelength around $\lambda \sim 2\pi a$, with a the grain radius. For $\lambda \ll 2\pi a$ the opacity becomes nearly constant while $\lambda \gg 2\pi a$ it drops. This effect is even stronger for the scattering opacity. The validity of this rule of thumb relies, however, on the grain size distribution itself. For the simple **Ivezic et al. (1997)** opacity law, it is only valid for grain size distribution powerlaws obeying **XXXXXXXXXXX**. [**TODO: Maybe here do an experiment with full opacity laws.**]

Acknowledgements. The authors acknowledge support by the High Performance and Cloud Computing Group at the Zentrum für Datenverarbeitung of the University of Tübingen, the state of Baden-Württemberg through bwHPC and the German Research Foundation (DFG) through grant no INST 37/935-1 FUGG. This research was initiated at the "Stars, Planets and Galaxies" meeting at the Harnackhaus in Berlin, April 2018. Part of this work was also funded by the DFG Forschergruppe FOR 2634 "Planet Formation Witnesses and Probes: Transition Disks".

References

ALMA Partnership, Brogan, C. L., Pérez, L. M., et al. 2015, ApJL, 808, L3

Andrews, S. M., Wilner, D. J., Hughes, A. M., Qi, C., & Dullemond, C. P. 2009, ApJ, 700, 1502
Andrews, S. M., Wilner, D. J., Zhu, Z., et al. 2016, ApJL, 820, L40
Barge, P. & Sommeria, J. 1995, A&A, 295, L1
Benisty, M., Stolker, T., Pohl, A., et al. 2017, A&A, 597, A42
Birnstiel, T., Dullemond, C. P., & Brauer, F. 2010, A&A, 513, A79
Brauer, F., Dullemond, C. P., Johansen, A., et al. 2007, A&A, 469, 1169
Casassus, S., van der Plas, G., M, S. P., et al. 2013, Nature, 493, 191
Chiang, E. I. & Goldreich, P. 1997, ApJ, 490, 368
Cieza, L. A., Casassus, S., Pérez, S., et al. 2017, ApJL, 851, L23
D'Alessio, P., Cantö, J., Calvet, N., & Lizano, S. 1998, ApJ, 500, 411
Demyk, K., Meny, C., Lu, X.-H., et al. 2017, A&A, 600, A123
Dong, R., Zhu, Z., Fung, J., et al. 2016, ApJL, 816, L12
Dubrulle, B., Morfill, G., & Sterzik, M. 1995, Icarus, 114, 237
Dullemond, C. P. & Dominik, C. 2004, A&A, 421, 1075
Dullemond, C. P., Dominik, C., & Natta, A. 2001, ApJ, 560, 957
Fedele, D., Carney, M., Hogerheijde, M. R., et al. 2017, A&A, 600, A72
Fedele, D., Tazzari, M., Booth, R., et al. 2018, A&A, 610, A24
Flaherty, K. M., Hughes, A. M., Teague, R., et al. 2018, ApJ, 856, 117
Fromang, S. & Nelson, R. P. 2009, A&A, 496, 597
Huang, J., Andrews, S. M., Cleeves, L. I., et al. 2018, ApJ, 852, 122
Isella, A., Guidi, G., Testi, L., et al. 2016, Physical Review Letters, 117, 251101
Ivezic, Z., Groenewegen, M. A. T., Men'shchikov, A., & Szczerba, R. 1997, MNRAS, 291, 121
Klahr, H. H. & Henning, T. 1997, Icarus, 128, 213
Kretke, K. A. & Lin, D. N. C. 2007, ApJL, 664, L55
Marino, S., Perez, S., & Casassus, S. 2015, ApJL, 798, L44
Pinilla, P., Benisty, M., & Birnstiel, T. 2012a, A&A, 545, A81
Pinilla, P., Birnstiel, T., Ricci, L., et al. 2012b, A&A, 538, A114
Pinte, C., Dent, W. R. F., Ménard, F., et al. 2016, ApJ, 816, 25
Powell, D., Murray-Clay, R., & Schlichting, H. E. 2017, ApJ, 840, 93
Ricci, L., Testi, L., Natta, A., et al. 2010, A&A, 512, A15
Testi, L., Natta, A., Shepherd, D. S., & Wilner, D. J. 2003, A&A, 403, 323
van der Marel, N., van Dishoeck, E. F., Bruderer, S., et al. 2013, Science, 340, 1199
Whipple, F. L. 1972, in From Plasma to Planet, ed. A. Elvius, 211
Youdin, A. N. & Goodman, J. 2005, ApJ, 620, 459
Youdin, A. N. & Lithwick, Y. 2007, Icarus, 192, 588

Appendix A: Steady-state dust distribution in a ringlike trap

A.1. Analytic approximate solution of dust trapping

Let us consider a narrow gas ring around the star at radius r_0 with a midplane pressure given by

$$p(r) = p_0 \exp\left(-\frac{(r-r_0)^2}{2w^2}\right) \tag{A.1}$$

where $w \ll r_0$ is the parameter setting the width of this gaussian gas ring. We assume that the gas is turbulent with turbulent diffusion coefficient D. Dust grains get trapped in this ring, and the dust will acquire a radial density profile that is in equilibrium between the radial dust drift pointing toward the peak of the gas pressure and radial turbulent diffusion pointing away from that position. The radial dust drift velocity is (see e.g. Birnstiel et al. 2010):

$$v_{\rm dr} = \frac{\rm St}{1+{\rm St}^2}\left(\frac{d\ln p}{d\ln r}\right)\frac{c_s^2}{\Omega_K r} \tag{A.2}$$

where c_s is the isothermal sound speed and the Stokes number St is defined as

$${\rm St} = \Omega_K t_{\rm stop} \tag{A.3}$$

where $t_{\rm stop}$ is the stopping time of the grains. The diffusion coefficient for the dust is (Youdin & Lithwick 2007):

$$D_{\rm d} = \frac{D}{1+{\rm St}^2} \tag{A.4}$$

We take D to be equal to the turbulent viscosity ν divided by the Schmidt number Sc, which we usually set to ${\rm Sc} = 1$. We use the usual α-prescription for the turbulence:

$$D = \frac{\nu}{\rm Sc} = \alpha_{\rm turb}\frac{c_s^2}{{\rm Sc}\,\Omega_K} \tag{A.5}$$

If D is sufficiently small, the dust will get concentrated into a ring with width w_d that is substantially smaller than the width of the gas ring w. In the following, we will ignore any terms arising from the curvature of the coordinates. The steady-state radial dift-mixing equation for the dust then becomes, in its approximate form:

$$\frac{d}{dr}\left(\Sigma_{\rm d} v_{\rm dr} - D_{\rm d}\frac{d\Sigma_{\rm d}}{dr}\right) = 0 \tag{A.6}$$

Integrating this equation once, with integration constant zero (which amounts to a zero net radial flux), yields

$$\Sigma_{\rm d} v_{\rm dr} = D_{\rm d}\frac{d\Sigma_{\rm d}}{dr} \tag{A.7}$$

From Eqs.(A.2,A.1) we can express $v_{\rm dr}$ as

$$v_{\rm dr} = -\left(\frac{c_s^2}{w^2\Omega_K({\rm St}+{\rm St}^{-1})}\right)(r-r_0) \tag{A.8}$$

With this expression we can solve Eq. (A.7) for $\Sigma_{\rm d}$, leading to the following simple analytic solution to the dust trapping problem:

$$\Sigma_{\rm d}(r) = \Sigma_{\rm d0} \exp\left(-\frac{(r-r_0)^2}{2w_{\rm d}^2}\right) \tag{A.9}$$

with

$$w_{\rm d} = w\sqrt{\frac{\Omega_K D_{\rm d}({\rm St}+{\rm St}^{-1})}{c_s^2}} = w\sqrt{\frac{\alpha_{\rm turb}}{{\rm Sc\,St}}} \tag{A.10}$$

The normalization constant $\Sigma_{\rm d0}$ can be approximately expressed in terms of the total dust mass trapped in the pressure bump:

$$M_d = 2\pi\int_0^\infty \Sigma_{\rm d}(r) r dr \simeq 2\pi r_0 \int_0^\infty \Sigma_{\rm d}(r) dr \tag{A.11}$$

which leads to

$$\Sigma_{d0} \simeq \frac{M_d}{(2\pi)^{3/2}\, r_0\, w_{\rm d}} \tag{A.12}$$

The approximation is best for narrow dust rings.

Note that this analytic solution is only valid as long as $\alpha_{\rm turb} \ll {\rm Sc\,St}$, or in other words as long as $w_{\rm d}$ is substantially smaller than w. This solution is, in fact, the radial version of the vertical settling-mixing equilibrium solutions of Dubrulle et al. (1995).

Unfortunately, the condition that $\alpha_{\rm turb} \ll {\rm Sc\,St}$ (and equivalently $w_d \ll w$) is easily broken for small grains and/or non-weak turbulence. This is similar to the case for vertical settling and mixing: Small grains tend not to settle below a few pressure scale heights. They settle down to some critical $z_{\rm settle}$, below which they are well mixed with the gas, and above which they are strongly depleted (Dullemond & Dominik 2004). Fromang & Nelson (2009) give an analytic solution to the settling-mixing problem (their Eq. 19) that reproduces the solutions of Dubrulle et al. (1995) for $\alpha_{\rm turb} \ll {\rm Sc\,St}$, but at the same time remains valid also for $\alpha_{\rm turb} \gtrsim {\rm Sc\,St}$, as long as $\alpha_{\rm turb}$, Sc and St remain constant with height above the midplane.

Given the similarity between the radial dust trapping problem and the vertical settling problem, one can show that the radial version of the solution of Fromang & Nelson (2009) reads:

$$\Sigma_{\rm d}(r) = \Sigma_{\rm d0} \exp\left[-\frac{{\rm Sc\,St}}{\alpha_{\rm turb}}\left(\exp\left(\frac{\Delta r^2}{2w^2}\right)-1\right) - \frac{\Delta r^2}{2w^2}\right] \tag{A.13}$$

where we defined Δr as

$$\Delta r \equiv (r - r_0) \tag{A.14}$$

The solution Eq. (A.13) is valid for any value of $\alpha_{\rm turb}/{\rm Sc\,St}$, as long as $\alpha_{\rm turb}$, Sc and St remain constant along the radial width of the dust trap, and as long as $w \ll r_0$, to prevent geometric terms from the cilindrical coordinates from dominating. One can easily verify that Eq. (A.13) reproduces the simpler Gaussian solution Eq. (A.9) for $\Delta r \ll w$. One can also verify that for $\alpha_{\rm turb} \gg {\rm Sc\,St}$ the shape of $\Sigma_{\rm d}(r)$ follows the shape of the gas pressure profile $p(r)$ (Eq. A.1).

The solution Eq. (A.13), like its simplified version Eq. (A.9), assumes that the dust is always near the midplane of the disk, so that one can ignore the vertical extent, and thereby ignore any variations in St. In other words, we assume that the vertical scale height of the dust layer h_d is much less than the gas pressure scale height h_p. As it turns out, this condition $h_d \ll h_p$ is satisfied if $\alpha_{\rm turb} \ll {\rm Sc\,St}$, which is the same condition that leads to $w_d \ll w$ (at least for ${\rm St} \ll 1$, which is what we assume). In fact, the radial dust ring width compared to the gas ring width is the same as the vertical dust layer thickness compared to the gas disk thickness:

$$\frac{w_d}{w} = \frac{h_d}{h_p} \tag{A.15}$$

In other words: the dust behaves radially the same way as vertically. The vertical dust settling can be regarded as dust trapping in vertical direction, or the radial dust trapping can be seen as radial settling of dust toward the pressure peak.

This also means that whenever the simplified Gaussian analytic solution (Eq. A.9) ceases to be valid, so does the simplified vertical Gaussian solution of Dubrulle et al. (1995). Or in other words, whenever the more sophisticated analytic solution Eq. (A.13) should be used instead of the simplified version, the assumption that the dust is settled near the midplane ceases to hold. Strictly speaking this invalidates Eq. (A.13), since this was derived under the assumption that the dust is all located near the midplane. But given that most of the dust mass is still close to the midplane, even for $\alpha_{\rm turb} \gtrsim {\rm Sc\,St}$, we are confident that Eq. (A.13) still remains approximately valid.

The typical shapes of the analytic dust surface density profiles is shown in Fig. A.1 for three different grain sizes from small to large. For the largest grains, which are the most strongly trapped near the pressure peak, and hence have the narrowest peak in Fig. A.1, the full analytic solution (Eq. A.13) nearly perfectly overlaps with the simplified (Gaussian) analytic solution (Eq. A.9). For large grains the simplified analytic solution is therefore sufficiently accurate. But in this parameter regime the dust rings are much narrower than the gas pressure bump ($w_d \ll w$).

For the tiny grains, which are well coupled to the gas, and hence have the widest peak in Fig. A.1, the dust trapping is very inefficient. Between 60 and 90 au the dust surface density follows nearly perfectly the shape of the gas bump, i.e. keeping the dust-to-gas ratio nearly constant. Only for $r \lesssim 60\,{\rm au}$ and $r \gtrsim 90\,{\rm au}$ the full solution drops below a constant dust-to-gas ratio. To good approximation one can thus say that a dust ring made up of these tiny grains has a width that equals the width of the gas pressure bump. Note that in this regime the simplified analytic model (Eq. A.9) fails miserably, as can be seen by the nearly horizontal green dotted curve in Fig. A.1.

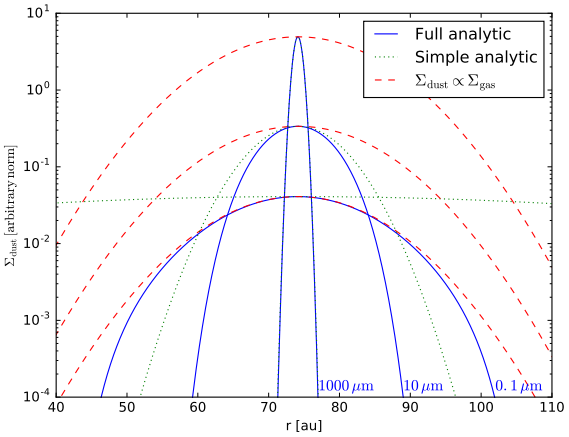

Fig. A.1. The analytic solution shown for three different grain sizes: small ($0.1\,\mu$m), middle middle ($10\,\mu$m) and large ($1000\,\mu$m). The normalizations of the three curves are arbitrary, optimized for clarity. The solid (blue) curves show the full analytic solution (Eq. A.13). The dotted (green) curves show the simplified analytic solution (Eq. A.9). The dashed (red) curves show the dust profile *if* the dust-to-gas ratio would be constant, which shows the shape of the gas pressure bump. The absense of the green dotted curve for the case of 1000 μm grains (the narrowest peak) is because for these large grains the simple analytic solution nearly perfectly overlaps with the full analytic solution. The parameters are chosen for AS 209, ring 1, with $M_* = 0.912\,M_\odot$, $T_{\rm gas} = 12.9\,$K. The gas surface density is taken to be $5\,{\rm g/cm^2}$ at the position of the ring, the turbulence parameter was set to $\alpha_{\rm turb} = 2 \times 10^{-4}$, the dust material density was chosen to be $2\,{\rm g/cm^3}$ consistent with slightly porous silicate dust aggregates. **[CHECK IF THIS IS CONSISTENT WITH THE OPACITY ESTIMATES, IN PARTICULAR THE RICCI OPACITY.]** The standard-deviation width of the gas pressure bump was set to $w = 9.7\,$au which equals two times the gas pressure scale height.

The intermediate size grains, corresponding to the intermediate curve (marked with $100\,\mu$m) in Fig. A.1, have a behavior between the above two extremes. The simplified analytic solution is a bit wider than the more accurate solution. The shape of the more accurate solution deviates from Gaussian. However, the deviation from Gaussian shape of the model is opposite to the deviation from Gaussian shape in the observations (Fig. 3). The observed data exceed the best-fit Gaussian in the flanks, while the model drops below the best-fit Gaussian in the flanks.

Whether this deviation from Gaussian is detectable in the ALMA data is, however, not so clear. For intermediate size grains the non-Gaussian profile can be easily mistaken for a Gaussian profile with a narrower width than both the gas bump and the simple analytic solution.

A.2. Resulting profiles for a size distribution

[THIS SECTION NEEDS HEAVY EDITING]

The analytic model of the dust trapping for a single grain size speaks for itself. But how does it look for a grain size distribution? Since the trapping width $w_{\rm d}$ for the different grain sizes is different, we can only impose the grain size distribution for the total (radially integrated) dust mass. We define the size distribution according to the following powerlaw

$$m(a)\frac{dN}{d\ln a} = \frac{dM}{d\ln a} \propto a^q \qquad \text{(A.16)}$$

where a is the grain size, $m(a)$ the corresponding grain mass, N the cumulative particle number and M the cumulative dust mass. The parameter q is the size distribution powerlaw coefficient, and it is $q = 1/2$ for the usual MRN distribution (this corresponds to $dN/da \propto a^{-3.5}$). We also need to define limits $a_{\rm min}$ and $a_{\rm max}$. The size distribution is then normalized such that its integral over $d\ln(a)$ is the total dust mass M. The radial surface density solution, Eq. (A.9), then becomes:

$$\frac{d\Sigma_{\rm d}(r)}{d\ln a} = \frac{1}{(2\pi)^{3/2} r_0 w_{\rm d}(a)} \frac{dM}{d\ln a} \exp\left(-\frac{(r-r_0)^2}{2w_{\rm d}(a)^2}\right) \qquad \text{(A.17)}$$

In Fig. A.2 we show the radial profiles for an MRN size distribution between $a_{\rm min} = 10^{-2}\,$cm and $a_{\rm min} = 1\,$cm and a total dust mass of $M = 1.3 \times 10^{-5}\,M_\odot$. The dust material density is taken to be $\xi_{\rm dust} = 2\,{\rm g/cm^3}$. We sample this size distribution with 10 grain sizes, evenly distributed in $\ln(a)$. These are the 10 curves in Fig. A.2. These surface densities are defined as being the local grain size distribution integrated over the width of the grain size bin: $\Sigma_{\rm bin} = \int_{\rm bin}(d\Sigma_{\rm dust}/da)da$. The stellar mass is $M_* = 0.9\,M_\odot$ and we set ${\rm Sc} = 1$.

MUST ALSO SPECIFY GAS DENSITY, TO GET STOKES NUMBERS. MUST SAY (AND CHECK) THAT EPSTEIN REGIME.

As expected, the largest grains are concentrated the most and the smallest ones the least. The largest grains, however, have the largest peak value of their surface density at the exact location of the gas pressure peak.

When it comes to the contribution to the optical depth, however, the situation looks a bit different. Let us assume a very simple dust opacity law, which roughly mimicks the real behavior of dust opacities: the model of Ivezic et al. (1997), where we take the scattering opacity zero for simplicity. In this simple but illustrative opacity model the cross section of a grain with radius a is the geometric cross section πa^2 for $2\pi a > \lambda$ (with λ the wavelength), while it is reduced by a factor $(2\pi a/\lambda)$ for $2\pi a < \lambda$. This means that for $2\pi a > \lambda$ the opacity (that is, the cross section per unit mass) is $\kappa = 3/4\xi_{\rm dust}a$ where $\xi_{\rm dust}$ is the material density, here taken to be $\xi_{\rm dust} = 2\,{\rm g/cm^3}$. For $2\pi a < \lambda$ this is reduced by a factor $(2\pi a/\lambda)$ and thus becomes independent of a.

It can be seen from Fig. A.3 that at the peak of the trap all grain sizes contribute equally to the optical depth.

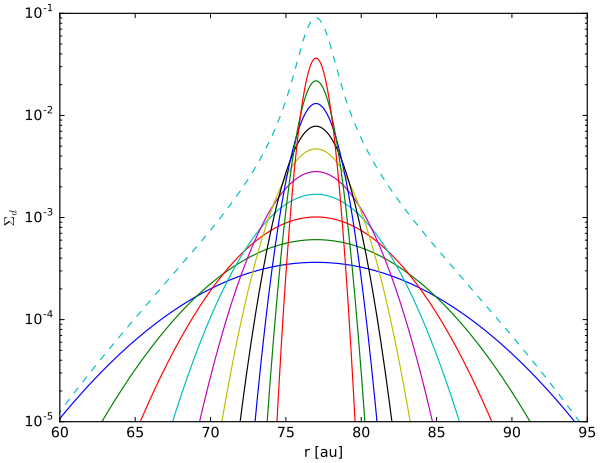

Fig. A.2. Results of the analytic dust trapping model for an MRN powerlaw grain size distribution between $a = 0.01\,\mathrm{cm}$ and $a = 1\,\mathrm{cm}$. The gas pressure bump has a FWHM of 70 au and a peak at $r = 77\,\mathrm{au}$. Shown here are the surface density profiles for 10 logarithmically binned grain sizes. The curve with the narrowest peak corresponds to a grain size of $a = 1\,\mathrm{cm}$, while that with the widest peak (and lowest maximum value) corresponds to a grain size of $a = 0.01\,\mathrm{cm}$. The intermediate curves correspond to $a = 0.0167$, 0.0278, 0.0464, 0.0774, 0.1291, 0.2154, 0.3593 and 0.5995 cm respectively. The dashed curve shows the total surface density of the dust, which is, by definition of the bin-integrated surface density, the sum of all 10 curves. For a description of the model setup and model parameters, see Section A.2.

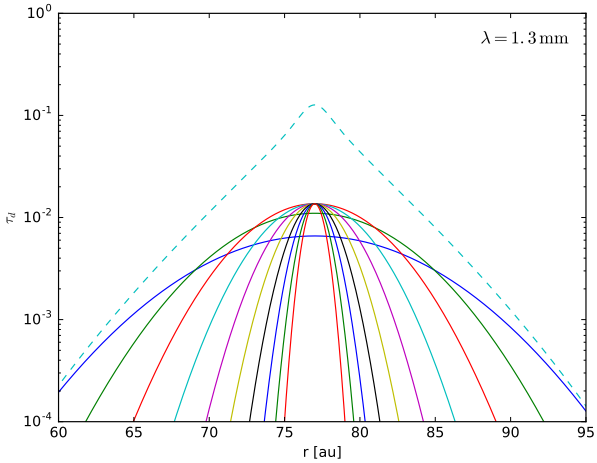

Fig. A.3. As Fig. A.2, but now the vertical optical depth at $\lambda = 1.3\,\mathrm{mm}$ (ALMA band 6) is shown. The opacity model of Ivezic et al. (1997) was used to compute these from the size distribution.

That is because, with our opacity model, the larger grains (the ones with $2\pi a > \lambda$) have an opacity equal to their geometric cross section per unit dust mass, which goes as $1/a$. The smallest grains (the ones with $a = 0.01$ and $a = 0.167$) have $2\pi a < \lambda$, which means that their opacity remains constant with a. Hence, for these two curves in Fig. A.3 the contribution to the peak optical depth drops below those of the other grains. Of course, with a more realistic opacity model this can change somewhat, but the rough principle remains valid.

More important is to notice that the relative contributions of the grain sizes to the peak optical depth may change if a different grain size distribution is chosen. Here we chose the MRN size distribution ($q = 1/2$), but that was a rather arbitrary choice. Given the complexity of the dust growth processes in protoplanetary disks, it is not at all said that the MRN distribution should be considered a preferred one. The reader may experiment with other values of q or entirely different grain size distribution shapes altogether.

A.3. Spectral slope variations across the ring

[TO DO]

A.4. Leakage and retention time of the dust in the traps

In our analytic model we have assumed that the pressure bump has a perfect Gaussian shape, meaning that the further away one goes from the peak of the trap, the steeper the pressure gradient (and thereby the faster the dust drift) becomes. This leads to perfect trapping: no dust can leak out of the trap. In reality the pressure bump has a finite radial width, and smoothly connects to the global disk structure. There will be a maximum pressure gradient at some distance away from the peak, and beyond that the pressure gradient declines again. If the width of the trapped dust is much narrower than this distance, virtually no dust will get lost out of the trap. But for small grains and/or strong turbulence, the width of the dust profile may be large enough that at the point of largest pressure gradient there is still a substantial amount of dust. Then the dust will leak out of the trap.

First make estimates based on current model. Then add the gas radial velocity by accretion.

A.5. Stability of gas ring

Here we must discuss how far into the wings of the gaussian is stable against RWI and other instabilities. Solberg-Hoiland stability criterion. A Gauss may not be very stabile in its flanks. This may limit the applicability of the full analytic solution.

A.6. Model degeneracies

When trying to infer the effectiveness of dust trapping within the rings with the analytic model of Section A.1, one notices that there are degeneracies in the possible combinations of parameters. Most obvious is the degen-

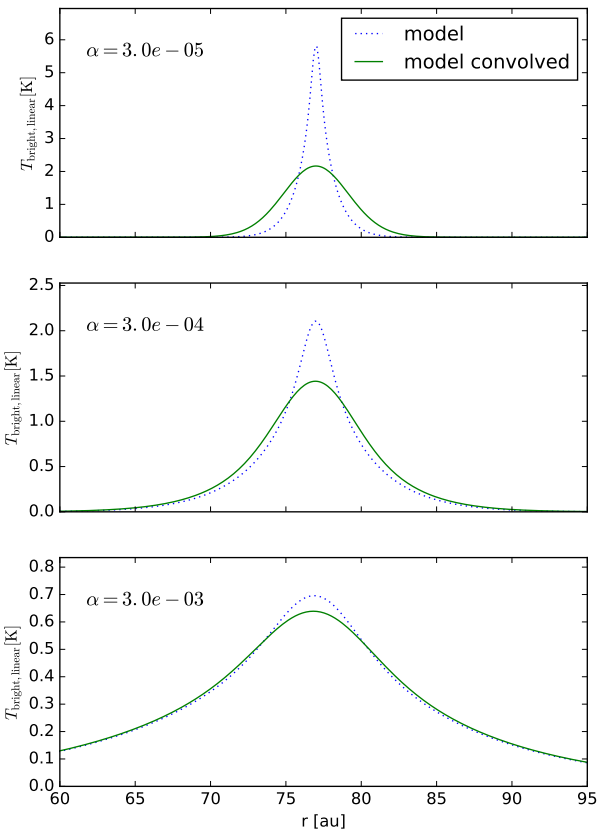

Fig. A.4. Results of the analytic dust trapping model for various turbulent strengths, for an MRN powerlaw grain size distribution between $a = 0.01$ cm and $a = 1$ cm. The gas pressure bump has a FWHM of 70 au and a peak at $r = 77$ au. Shown here is the predicted brightness temperature at a wavelength $\lambda = 1.3$ mm before (dashed) and after (solid) convolution with the ALMA beam, assuming a source distance of $d = 126$ pc. For a description of the model setup and model parameters, see Section **??**.

eracy between grain size and turbulence: smaller grains and stronger turbulence may yield the same dust trapping width. But also the width of the gas pressure bump can be compensated: a narrower bump but stronger turbulence (or smaller grains) will yield the same ring width.

[CONTINUE THIS; SOME DEGENERACIES FOLLOW DIRECTLY FROM THE EQUATIONS.]

A.6.1. Could the rings be optically thick at the center?

All rings in our sample show sub-Planckian brightness, at least for the disk temperature assumed in our model. We have calculated the disk midplane temperature using a simple "flaring angle recipe". If the disks are, however, substantially colder (by up to a factor of 2.5 to 3) then the peak flux of the rings might be consistent with saturated emission, i.e. emission expected from an optically thick disk. So the question is: how sure are we that the rings are sub-Planckian?

To reduce the midplane temperature by a factor of 2 the irradiation flux must be reduced roughly by a factor of $2^4 = 16$. Within the flaring angle recipe this would lead to unrealistically low flaring angle. Presently we assumed $\varphi = 0.02$, so that it would have to reduce to $\varphi = 0.0013$, which is so low that we can no longer trust the flaring angle recipe. However, maybe the outer disk lies in the shadow of the inner disk. To see whether this can reduce the temperature to low enough values, we perform a proper radiative transfer calculation. The results are shown in Appendix (**XXXX**). It shows that **XXXXX**.

There is another issue, however. If the emission saturates to the optically thick brightness, i.e. to the Planck function, then the radial profile of the ring should be flat-topped. This is clearly not what we see in the rings in our sample, with the possible exception of the ring of GW Lup which shows a very slight hint of that. In general, however, it seems that the simple picture of collecting so much dust into the ring that the ring becomes optically thick does not seem to explain the observed radial brightness profiles. On the other hand, optical thickness can also occur on smaller scales, as we will discuss in Section 4.

Appendix B: Gauss fitting procedure

In this paper we study each dust ring individually, and try to understand it in terms of the trapping of dust in a pressure trap. In Appendix A we find that for a Gaussian pressure bump the solution to the radial dust mixing and drift problem is, to first approximation, also a Gaussian, albeit a narrower one. Fitting the dust trapping model to the data can therefore be done in two stages: first fitting a Gaussian radial profile to the observed rings, then interpreting these Gaussian fits through the dust trapping model. In this appendix

Appendix C: Computing the dust mass trapped in the rings

We can compute the dust mass trapped in each of the rings by integrating over the measured brightness temperature profiles. However, the profiles do not go down to zero far way from the peak, and so it is not well defined what belongs to the ring and what not. Instead, we will compute the dust mass from the Gaussian profile that is fitted to the ring emission. This will slightly underestimate the dust mass, because the excess emission in the flanks of the profiles (see Fig. 3) will not be included. But there are far more serious issues to worry about, such as our limited knowledge of the disk temperature, the uncertainties of the dust opacities, as well as optical depth effects. So we will estimate the mass of the best fitting Gaussian model only.

We will assume that the intrinsic dust temperature is as given in Table 2 (column T_d), which was computed based on a simple flaring angle irradiation model. We consider the Gaussian profile with the deconvolved width, i.e. w_d (not σ). The peak linear brightness temperature is taken to be

$$A_\mathrm{deconv} = \frac{\sigma}{w_d} A \tag{C.1}$$

where A, σ and w_d are from Table 2. We do not account for geometric terms in the deconvolution, which is justified as long as $\sigma \ll r$. The deconvolved Gaussian brightness profile is then

$$T_\mathrm{br,lin,deconv}(r) = A_\mathrm{deconv} \exp\left(-\frac{(r-r_0)^2}{2w_d^2}\right) \tag{C.2}$$

Next we have to worry about optical depth effects. From Table 2 one can see that for most rings A_deconv is significantly smaller than $T_\mathrm{d,br,lin}$. However, for the rings of AS 209 the ratios $A_\mathrm{deconv}/T_\mathrm{d,br,lin}$ are around 0.5, so optical depth effects start to play a role. Given a dust surface density profile $\Sigma_\mathrm{d}(r)$ as a function of radial coordinate r, and given an absorption opacity κ_a at the wavelength we are measuring, the absorption optical depth $\tau_\mathrm{a}(r)$ is

$$\tau_\mathrm{a}(r) = \Sigma_\mathrm{d}(r)\kappa_\mathrm{a} \tag{C.3}$$

We assume that scattering does not play a role. The emission from this dusty ring is then, expressed as linear brightness temperature:

$$T_\mathrm{br,lin,deconv}(r) = \left(1 - e^{-\tau_\mathrm{a}(r)}\right) T_\mathrm{d,br,lin} \tag{C.4}$$

If $\tau_\mathrm{a}(r) \ll 1$ for all r this reduces to

$$T_\mathrm{br,lin,deconv}(r) = \tau_\mathrm{a}(r)\, T_\mathrm{d,br,lin} \tag{C.5}$$

But given that for some rings $A_\mathrm{deconv}/T_\mathrm{d,br,lin} = \max(I_\mathrm{obs}(r)/B_\nu(T_\mathrm{d}))$ can be as large as ~ 0.5, this condition is not always fulfilled. On the other hand, these optical depth effects cannot be too strong, because then the Gaussian shape would flatten off at the top, which is not what we see in the observations. We will therefore continue our computation without accounting for these (mild) optical depth effects. This will lead to a slight underestimation of the mass. The reader can estimate the magnitude of this underestimation by comparing $(1 - \exp(-\tau_\mathrm{a}))$ to τ_a.

Using Eq. (C.5) we can, from the deconvolved $T_\mathrm{br,lin,deconv}(r)$ (Eq. C.2), solve for $\tau_\mathrm{a}(r)$ and obtain

$$\tau_\mathrm{a}(r) = \frac{A_\mathrm{deconv}}{T_\mathrm{d,br,lin}} \exp\left(-\frac{(r-r_0)^2}{2w_d^2}\right) \tag{C.6}$$

leading with Eq. (C.3) to

$$\Sigma_\mathrm{d}(r) = \frac{A_\mathrm{deconv}}{\kappa_\mathrm{a} T_\mathrm{d,br,lin}} \exp\left(-\frac{(r-r_0)^2}{2w_d^2}\right) \tag{C.7}$$

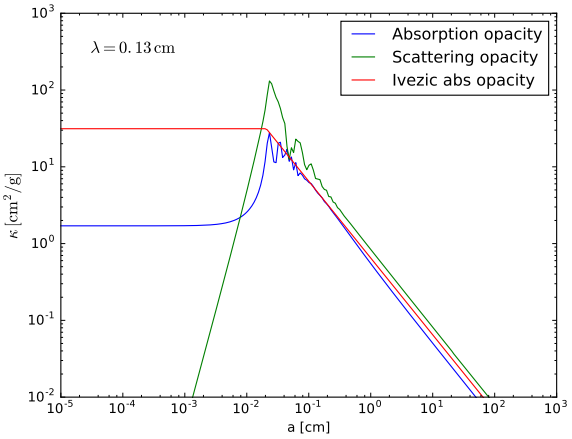

Fig. C.1. The dust opacity at $\lambda = 0.13\,\mathrm{cm}$ as a function of the grain radius a. Plotted are the absorption opacity of Ricci et al. (2010), the corresponding scattering opacity, as well as the analytic absorption opacity of Ivezic et al. (1997).

Integrating over r, ignoring geometric terms leads to

$$\begin{aligned} M_\mathrm{d} &\simeq 2\pi r_0 \int_{r_\mathrm{in}}^{r_\mathrm{out}} \Sigma_\mathrm{d}(r) dr \\ &= (2\pi)^{3/2} \frac{r_0 w_d A_\mathrm{deconv}}{\kappa_\mathrm{a} T_\mathrm{d,br,lin}} \\ &= (2\pi)^{3/2} \frac{r_0 \sigma A}{\kappa_\mathrm{a} T_\mathrm{d,br,lin}} \end{aligned} \tag{C.8}$$

As the final step we have to make an estimate of the absorption opacity κ_a. This is the biggest uncertainty because it is not well understood what the composition of the dust is, what the grain sizes are and what the effect of the geometry is on the opacity. We will use two estimates: on the one hand we will employ the opacity used by Ricci et al. (2010), which is a mixture of astronomical silicate and amorphous carbon (see Fig. C.1). On the other hand we will use the dummy opacity model of Ivezic et al. (1997). These two opacities serve as two extremes that bracket the likely true value. It is known that at long wavelengths the opacities computed with the Mie procedure from laboratory measured optical constants are likely to be underestimates by up to a factor of 10 (Demyk et al. 2017). The more realistic opacities of (Demyk et al. 2017) are in between our two bracketing opacities. For the mass estimate we use the opacity at $\lambda = 0.13\,\mathrm{cm}$ for small grains ($a = 1\mu\mathrm{m}$). For the Ricci opacity this is $\kappa_\mathrm{a,ri} = 1.70\,\mathrm{cm}^2/\mathrm{g}$, while for the Ivezic opacity this is $\kappa_\mathrm{a,ri} = 31.3\,\mathrm{cm}^2/\mathrm{g}$. The masses estimated from Eq. (C.8) using these two bracketing opacities are listed in Table 3. Note that the opacity of Ricci et al. (2010) has a peak around a grain size of 2 mm. That peak value happens to be very close to the Ivezic value of $31.3\,\mathrm{cm}^2/\mathrm{g}$. We can thus also regard the Ivezic mass estimate to be the mass if all grains have a radius of 2 mm.